

Statistical properties of shear deformation of granular media and analogies with natural seismic processes ¹

Mykulyak S.V.², Polyakovskiy V.V.³, Skurativskiy S.I.⁴

Subbotin institute of geophysics, Nat. Acad. of Sci. of Ukraine
Bohdan Khmelnytskyi str. 63-G, Kyiv, Ukraine

Abstract. In this paper, the process of shear deformation of the medium formed by the cubic grains is investigated experimentally. It is demonstrated that the deformation process is intermittent and accompanied by the radiation of acoustic perturbations. These perturbations obey statistical laws that are inherent in natural seismic processes: the frequency-energy scaling relation (the Gutenberg-Richter law) and the generalized Omori law for temporal decay of aftershocks. The weak perturbations influence on the process of shear deformation is studied for the mono-dispersed medium. During the granular medium stimulation by weak periodic signals, the existence of a critical frequency providing the smallest number of critical events in the granular medium is identified. We also developed the algorithm providing smaller stresses inside the granular massif by means of external perturbations during shear deformation. Taking into account the statistical similarity between shear and seismic processes, these results open prospects for the ability to affect the natural seismic processes.

Keyword: Granular media; Shear; Self-organized criticality; Seismic processes

1 Introduction

The rock massifs forming the lithosphere are extremely diverse, but there is an important characteristics of rocks that is inherent in almost all of them: it is discreteness [6]. Discreteness is observed in a wide range of scale levels: for instance, the grains in rocks, the size of which is millimeters or their fraction; the pieces of rock that can be observed in quarries or mountains with centimeters or meters in size; the tectonic blocks having the dimensions of tens and hundreds of kilometers, the largest structural elements of Earth's crust – tectonic plates extended over thousands, or even tens of thousands of kilometers [1–6]. Block structuration is most brightly manifested on the boundaries of tectonic plates, where the rock materials were destroyed by earthquakes for a long time [7–13].

According to the concept proposed by Sadosky et al. [6], the geophysical medium is a thermodynamically open system consisted of hierarchically embedded blocks. In this system, the long-range spatial and temporal correlations take place causing the emergence of dynamical localized structures and other phenomena of self-organization. In particular, the dynamic behavior of the seismically active area is similar to the behavior of a system in the

¹Published in *Pure and Applied Geophysics* (2019) <https://doi.org/10.1007/s00024-019-02209-0>

²e-mail: mykulyak@ukr.net

³e-mail: polykovskiyvo@nas.gov.ua

⁴e-mail: skurserg@gmail.com

state of self-organized criticality (SOC) [14–16]. A number of models were elaborated that reproduce the behavior of seismic areas as being in the SOC state [17–31]. In particular, the hierarchical block model taking the SOC state of seismic region into account is developed in [32].

It is worth noting that similar properties are also endowed with granular media under shear deformation [13]. Experimental studies and computer simulation of deformation of granular massifs indicate that fluctuations of intergranular forces and velocities of granules can many times exceed their mean values [33–36] that is common to seismic processes [15] as well. During the deformation of granular systems, the long-range correlations [37] are intensified. Moreover, the displacement of granular media occurs intermittently [34,35,38,39] and is accompanied by the radiation of stochastic acoustic disturbances. Investigation of these regularities and granular media responses on external influences are important for understanding the discrete media behavior taking place at different scales, in particular on the scale associated with the earthquakes generation.

In this paper, we investigate experimentally the shear deformation of granular medium consisted of cubic grains. Section 2 contains the experimental rig description. In Section 3 the influence of additional massif load on the deformation process and statistical properties of acoustic emission released by considered granular system are studied in more detail. In Section 4 it is examined the shear processes in granular medium when the periodic and impulse external disturbances are applied. The final section contains the concluding remarks. Notably, from the foregoing provisions it follows that the behavior of this system is similar to the behavior of the geomedium in a seismic zone. Therefore, such studies may help in understanding the unknown properties of natural seismic processes and possibility of artificial influence on them.

2 Experimental installation for the study of shear deformation of massif formed from cubic grains

The study of shear deformation process of granular media was carried out for both cases of external perturbations and their absence. The experimental installation is the box, which is made from plexiglass and consists of lower fixed part and upper slider one (Fig. 1). The lower box part has the following internal sizes: the length along shear direction 0.3 m, the height 0.07 m, and the width 0.2 m. The front and back wall thickness is 0.1 m. The slider part is of the same dimension. The grinding of contact surfaces between lower and upper box parts was performed. To provide the directional sliding of the upper part, the guide plates were installed on the lower part. In turn, the slider part of the device is equipped with the limiters prohibiting the movement in the vertical direction. The piston (2) that can move freely in a vertical direction is located on the granular massif.

The movement of the slider block is carried out using a traction mechanism (4) providing the slider block displacement 0.1 m in a minute. This device consists of a gear motor NMRV 090/040, which is connected to the rope shaft. One end of the rope (6) is attached to the shaft, and the other to the force sensor KMB 19 (5), which is tightly tied to the leading edge of the upper box.

On the slider part there are three single axis accelerometers T-500 (7) measuring the accelerations in three orthogonal directions. The force sensor (5) on the leading edge measures

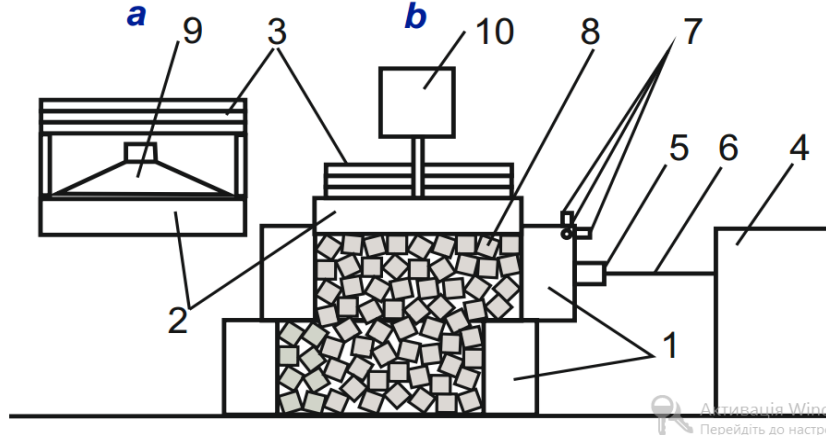


Figure 1: The sketch of experimental setup. Designations : 1 – box consisting of two parts, 2 – piston, 3 – load, 4 – traction mechanism, 5 – force sensor, 6 – rope, 7 – accelerometers, 8 – cubic grains, 9 – acoustic speaker, 10 – impulse generator. The module (a) is used in the case of periodic action on the granular medium, whereas (b) is applied for producing the impulse action.

the granular massif reaction on the shear deformation.

The study of external perturbations influence on the granular medium shear is carried out for two types of actions: a) periodic and b) impulse. In the first case, the module (a) consisting of piston (2), load (3) and acoustic low-frequency speaker 75-GDN-4 (9) is used. The speaker generates the periodic weak disturbances with 10 Watts power in the frequency range of 50-1000 Hz.

To investigate the impulse perturbations influence on the shear process, instead of the module (a), the module (b) is used. The perturbations are generated by an impulse generator (10) mounted on the upper surface of the piston (2). There is also possibility to vary the static loading (3).

3 The characteristics of granular medium reaction on shear deformation

In the first series of experiments, let us consider how the magnitude of static loading of the granular medium affects the process of its shear deformation. The experimental set-up is used with the module (a) when the acoustic speaker (9) is turned off.

Monodisperse granular medium is formed by the massif of 3000 cubic grains made of plexiglass with the following characteristics: Young's modulus is $E = 3 \cdot 10^9$ Pa, Poisson's ratio is $\nu = 0.3$, and density $\rho = 1200$ kg/m³. The coefficient of friction between the surfaces of the grains is $k = 0.4$. Initially, the grains fill the volume of the box in such a way that the piston is immersed in the box at the depth of 0.4 mm. Thus, the packing fraction (solid volume fraction) of the granular medium is $\gamma = 0.368$.

According to the estimates [40], the average size of blocks in the area of San Andreas fault in California is about 90 km and the width of the area, where the main deformation occurs

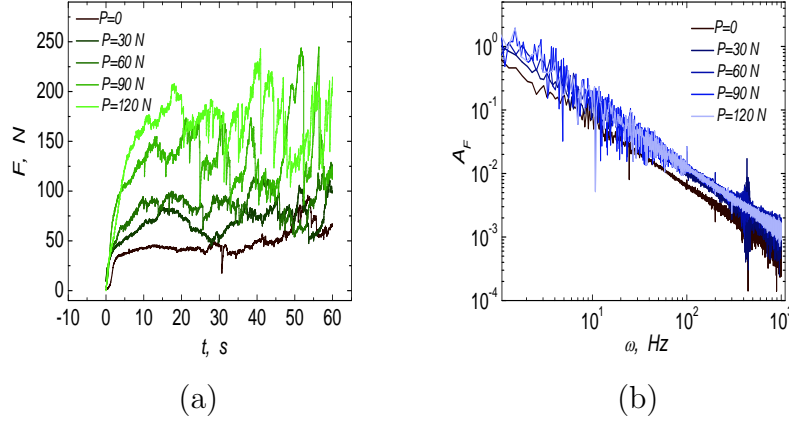


Figure 2: Temporal dependences (a) of the force F at loading $P = 0, 30, 60, 90, 120$ N (curves from bottom to top) and their Fourier spectra (b).

between the tectonic Pacific plate the North American plate, is 565 km. Thus, the ratio of the area width to the block size is about $\kappa \approx 6$. This ratio belongs to the interval 5-10 of the ratio κ observed in experiments with a shear deformation of the granular medium [41]. In our case reduced width of the granular massif is about 14, which is close to the shear band width. The packing fraction of the monodisperse granular medium is $\gamma = 0.368$. This packing fraction value is less than critical one ($\gamma = 0.5$) when the crystallization appears [42]. Under natural conditions, crystallization is unlikely also, as the discrete medium formed by geoblocks is not monodisperse.

The temporal dependence of the traction force $F(t)$ registered with the force sensor is depicted in Fig. 2a. Analysis of these dependencies indicates a tendency to increase the force of reaction F with increasing loading on the piston. Performing the discrete Fourier transform of temporal $F(t)$ dependences, the corresponding spectra of these dependencies are obtained (Fig. 2b). All spectra are similar and obey the power relations. The estimation of the slope of regression line for the data in Fig. 2b gives the degrees of power which are close to each other and are equal to about -0.998 ± 0.003 . This points to the similarity of processes at different loading, as well as to the scale invariance of the shear deformation process.

During medium deformation the acceleration $a(t)$ in acoustic waves generated by the medium is examined. We measure all components of $a(t)$ with accelerometers (7) (Fig. 1). The inset in Fig. 3a shows the part of the signal $a_y(t)$ in the interval $t \in [49.78; 49.80]$ s recorded by the accelerometer in the direction of movement of the upper device part. This signal is a sequence of perturbations generated by the granular system. Each component a_f , $f = \{x, y, z\}$ is integrated in order to obtain the temporal dependence of the velocity component v_f .

To distinguish between individual pulses we have used an autoregressive-Akaike information criteria (AR-AIC) picker [43, 44].

Next, let us introduce the quantities

$$e_i^* = \frac{1}{t_i^e - t_i^b} \int_{t_i^b}^{t_i^e} \sum_{x,y,z} v_f^2(t) dt, \quad (1)$$

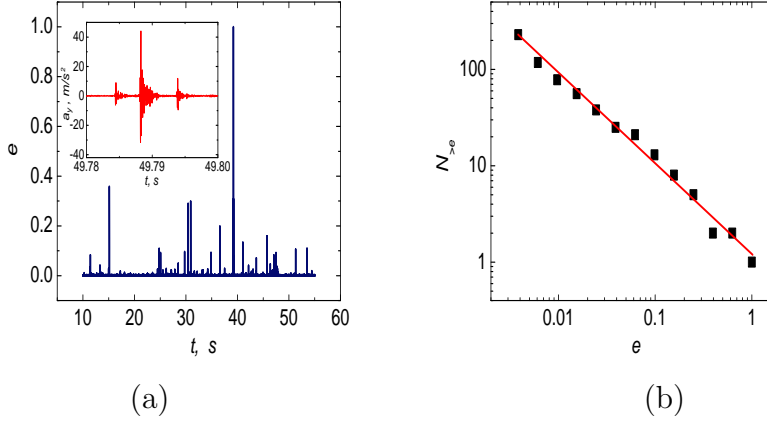


Figure 3: Sequences (1) of acoustic perturbation energy depending on time (a) and corresponding cumulative complementary distribution (square dots) of perturbations by energy (b) and its approximation by power relation (solid line). The inset in left panel is the profile of a_y -component for the acceleration.

where t_i^b and t_i^e are the initial and final moments of the i th perturbation, i.e. the boundaries of separate pulse (the inset in Fig. 3(a)). These quantities are proportional to the energies [45] of the perturbations. As a result, we obtain the sequence $e_i = e_i^* / \max(e_i^*)$ which can be regarded as a sequence of reduced energies of acoustic perturbations.

In particular, the sequence e_i for the experiment when the loading on a box cover is $P = 120$ N is shown in Fig. 3(a). Now the question arises: does this sequence obey the statistical laws that take place for seismic processes?

At first, consider the cumulative complementary distribution of acoustic perturbations for energies. It can be approximated by the power relation

$$N(> e) = C e^{-\beta}, \quad (2)$$

where $\beta = 0.93 \pm 0.03$, $C = -4.88 \pm 0.04$. From Fig. 6(b) it follows that the approximation matches the experimental distribution. Therefore, this distribution is of power nature as Gutenberg-Richter's law [46]. Moreover, the index β belongs to the interval 0.8-1.05 which is typical for seismic processes [21].

The statistics of foreshocks [47] and aftershocks [48] caused by earthquakes is an important characteristics of seismic zones and their dynamics. Consider analogous phenomena associated with large emission of energy exceeding the threshold $e_{th} = 0.02$ (Fig. 4a). It turns out, model aftershocks attenuate according to the Omori law [48] which is valid for natural aftershocks of large earthquakes [49]:

$$N = \frac{k}{(t + c)^p},$$

where the coefficients $k = 0.13 \pm 0.03$, $c = 0.01$, $p = 0.91 \pm 0.06$ (Fig. 4b). The presence of foreshocks and aftershocks testifies to the existence of temporal correlations in the process of generation of perturbations.

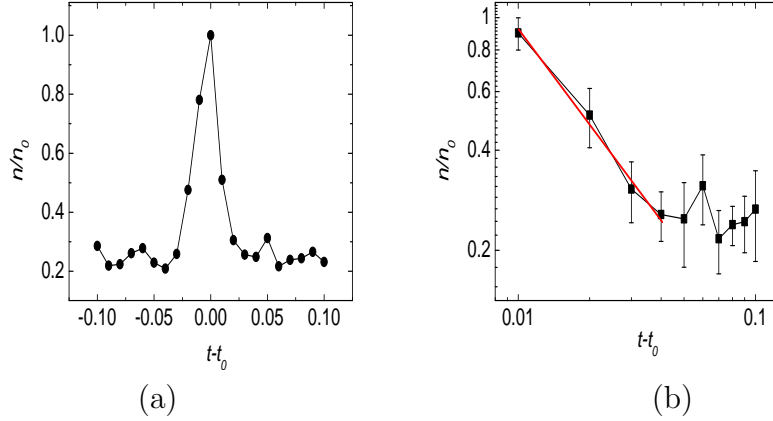


Figure 4: Dependence of the average number of acoustic disturbances on time to a major earthquake (a); power approximation of aftershocks (b). Here n_0 stands for the number of main shocks, n is the total shock number, and the 95% confidence intervals are shown.

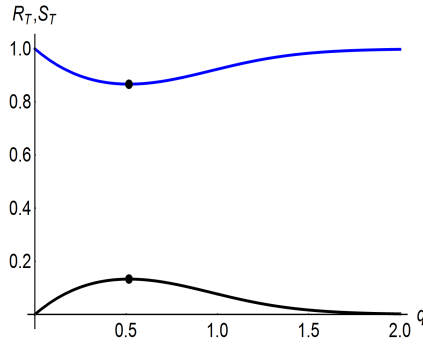


Figure 5: The estimation of the entropy index q . The functions R_T (upper curve) and S_T (lower curve). The extremum abscissa is $q = 0.516$.

The nature of the observed experimental data can be examined by using the generalized entropy conception [50–63]. This extension of thermodynamics and statistical physics introduced by Tsallis [64] deals with the nonergodic systems and leads to the nonextensive thermodynamics and statistical mechanics. Instead of classical entropy, the quantity S_T is defined

$$S_T = \frac{1 - \sum_{i=1}^Q p_i^q}{q - 1}, \quad q \in R,$$

where q is the Tsallis (or entropy) index, $\sum_{i=1}^Q p_i = 1$. Note that the limit $q \rightarrow 1$ corresponds to the Boltzmann-Gibbs entropy $S_T \rightarrow -\sum_{i=1}^Q p_i \ln p_i$ and the deviation of q from 1 points to the appearance of long-range correlations. It has been shown that at $q < 1$ the physical system behavior depends on rare events, whereas at $q > 1$ the frequent events have more weight [65].

To estimate the index q , the approach proposed in [66] is used. According to this method, the maximum entropy principal on the base of S_T is applied. The auxiliary function known

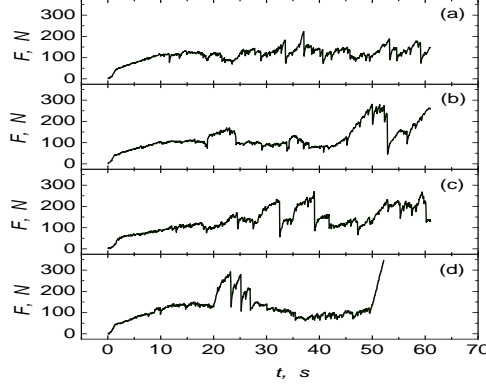


Figure 6: Temporal dependences for the traction force F when the medium is monodisperse: identical cubes of size 10 mm (a) and polydisperse: the mixture of cubes of sizes 10 mm and 25 mm in proportions: b – 80% \times 20% (number of grains: 2400 \times 38), c – 70% \times 30% (2100 \times 59), d – 50% \times 50% (1500 \times 96).

as redundancy R_T is defined

$$R_T = 1 - \frac{S_T}{S_{T_{\max}}},$$

where $S_{T_{\max}} = \frac{1-Q^{1-q}}{q-1}$ is the maximum of the function S_T which is reached on the equiprobable microstates $p_i = 1/Q$.

We thus construct the functions S_T and R_T using the sequence e_i presented in Fig. 3a. Each of these functions possesses single extremum depicted in Fig. 5 with the filled circles. The numerical estimation of extremum coordinates gives $q = 0.516 < 1$. This means that the process described by this distribution possesses long-range correlations and the system dynamics is defined by the mutual influence of a large number of rare events.

The next series of experiments is concerned with the study of influence of medium's heterogeneity on its deformation. To do this, the mixture of cubic grains of two sizes $l_1 = 10$ mm and $l_2 = 25$ mm is used. The shear deformation performs at loading $P = 60$ N. Temporal dependences of the traction force (Fig. 6) show that the process of deformation of both monodisperse and disperse media is not significantly different. This is also confirmed by the comparison of their Tsallis indexes which are practically unchanged for the mixtures of cubes. However, when number of grains with the edge $l_2 = 25$ mm increases, the stress increases as well. Note that if the bulk ratio of cubes of different volumes equals 0.5, the significant increase in traction force takes place leading to the rope destruction (Fig.6d).

4 Influence of external perturbations on shear deformation

According to the studies presented above, the behavior of the granular medium in the process of shear deformation is enriched by complicated stochastic reactions to shear loading. This response of the system obeys the statistical laws that are inherent in the natural seismic

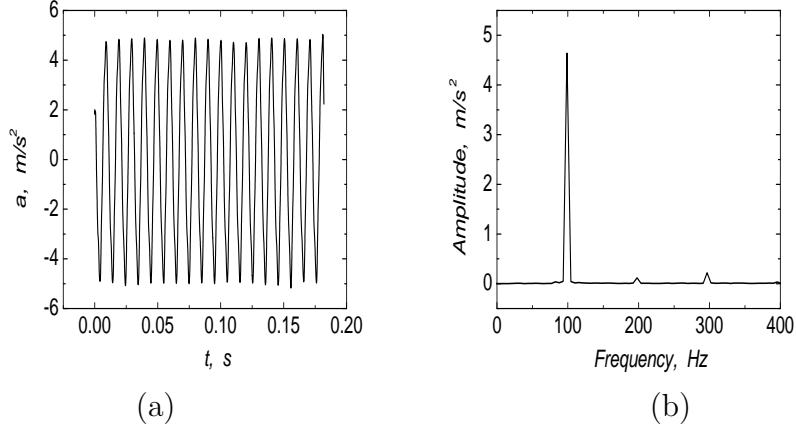


Figure 7: The signal recorded by the accelerometer at the bottom of the piston (a) and its spectrum (b).

process. The question arises whether it is possible to make a change in the behavior of this complex system with the help of small disturbances?

As above, let us consider the shear deformation of the granular medium formed by 3000 cubes of the size $l_1 = 10$ mm. The displacement is carried out with the device described in Fig.1. The *periodic* perturbations of the 50-1000 Hz frequency range are injected into the medium with the help of acoustic speaker mounted in the module (a). The massif is stressed by the load $P = 60$ N.

To check what kind of signal is entered the medium, an additional accelerometer is installed in the bottom of the piston. Fig. 7a shows the accelerations, measured by this sensor, and its Fourier spectrum at the 100 Hz frequency of input periodic signal (Fig. 7b). There is the main maximum in the diagram, whereas the spectral amplitudes of other harmonics are insignificant. Similar spectra have signals received for input periodic perturbations at frequencies of 50, 300, 500, 1000 Hz. From this it follows that the signal passing through the piston is almost not distorted.

Thus, after supporting explanations, let's return to the process of deforming under the action of traction force F . To analyze the influence of external perturbations, jumps of force are calculated as the difference between adjacent local maxima and minima. These jumps of force are associated with the reaction of the block media to the shear. The constructed distributions of the number of jumps at their intensity for the five frequencies of periodic perturbations are shown in Fig. 8a. From this figure it follows that these distributions are close to power functions and depend on the frequency of perturbations. The dependence of the power index on the frequency is shown in Fig. 8b. It turns out that at a 500 Hz frequency the index has a local maximum. That is, at this frequency, the number of large jumps of force is the smallest. In addition, the maximum values of jumps are the smallest among all frequencies. This allows us to conclude that under these conditions the deformation process is the most smooth and "soft", without sharp jumps of force.

This feature of the parameter β behaviour encourages us to evaluate the Tsallis indexes for corresponding force distributions. The application of the technique described above results in the graph plotted in Fig. 8b (bottom panel). We see that the minimum value of q is reached

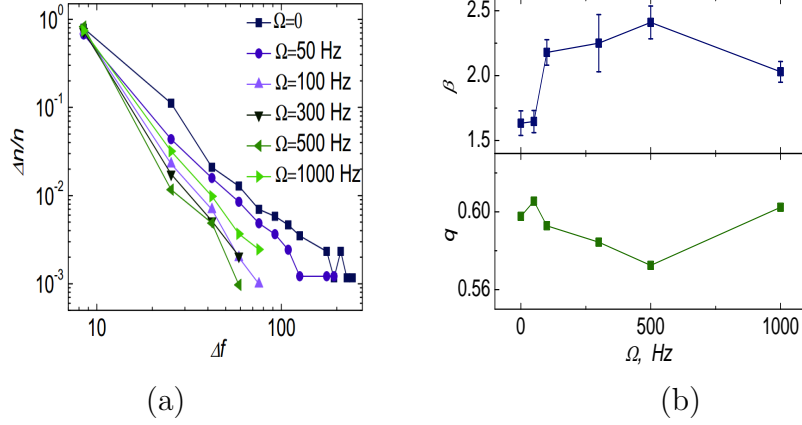


Figure 8: The distribution of force jumps at different values of perturbation frequencies Ω (a), the power index β (upper panel) in the approximation of distributions and Tsallis index q (bottom panel) versus the frequency of perturbation Ω (b).

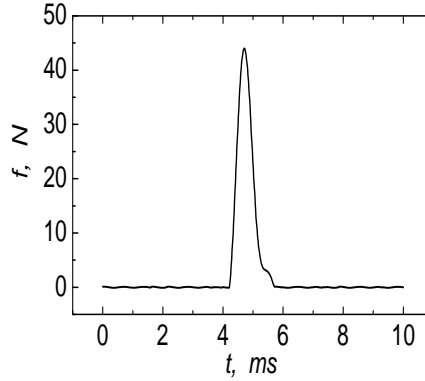


Figure 9: The pulse shape of signal generated by the impulse generator.

at the same frequency $\Omega = 500$ Hz.

The next series of experiments is concerned with studies of influences of external *impulse* perturbations on the shear process. In this case the impulse generator (10) (the module (b), Fig.1) is used in order to send the signal in the medium when the traction force reaches some threshold value F^* . The signals are sent with the frequency 1 Hz as long as the condition $F \geq F^*$ is fulfilled. Figure 9 shows the shape of one of the force impulses generated by the generator. The amplitude of the pulse is $f^m = 44$ N, lasted for $\tau = 1$ ms. The granular medium consists of 3000 cubes of the 10 mm sizes. In all experiments the medium is loaded with the weight of $P = 60$ N. The experiments are carried out at $F^* = 200, 150, 125$ N.

The temporal dependencies of the traction force for these three threshold values are plotted in Fig.10, which also shows the temporal dependence without external action. From this figure it follows that acting on the medium with external perturbations can avoid large tensions. It should be noted that the reduction of the traction force to a value smaller than the threshold value is not achieved by a single strike. This is well illustrated by Fig. 10b,

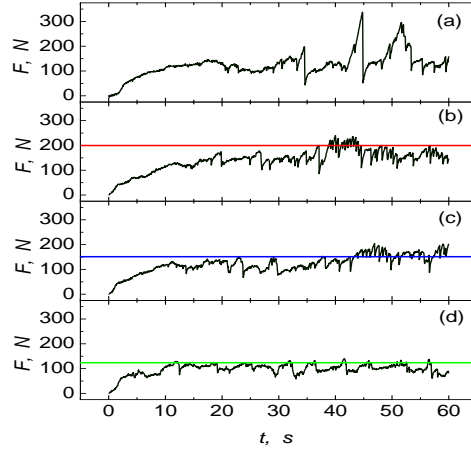


Figure 10: Time dependencies of the traction force $F(t)$ during shear deformation of massif loaded by the force $P = 60\text{N}$ and stimulated by periodic signals of magnitude $f^m = 44\text{N}$ when it is chosen the different threshold values: $F^* = 200\text{ N}$ (b), $F^* = 150\text{ N}$ (c), $F^* = 125\text{ N}$ (d). For comparison, the profile of $F(t)$ without external action (a).

c, where the perturbations are repeatedly sent in the medium. The experiments indicate that the use of such a mechanism makes the process of shear deformation smoother and that occurs at lower stresses.

These considerations are also accompanied by the Tsallis index evaluation. For the threshold values $F^* = \{0; 125; 150; 200\}\text{N}$, it is obtained the indexes $q = \{0.591; 0.604; 0.603; 0.587\}$, which are almost similar to each other.

5 Concluding remarks

Summarizing, it should be noted that experiments on the shear deformation of the granular medium exhibited statistical similarity with natural seismic processes. The acoustic perturbations released by the granular medium during shear deformation obey the power-like distribution similar to Gutenberg-Richter's law. It turned out that the power index lays in the range which is typical for natural earthquakes. Moreover, for large acoustic disturbances the foreshocks and aftershocks were observed as well. It was shown that model aftershocks attenuate in accordance with the power law with the index close to 1, i.e. Omori's law, that coincides with the statistical properties of seismic process.

It is also shown that the sequence of energies of acoustic disturbances is characterized by the Tsallis index $q = 0.516 < 1$. This testifies about the presence of long-range correlations in the shear motion and the system dynamics is defined by the mutual influence of a large number of rare events.

Our experiments with different loads revealed the similarity of processes of shear deformation, as well as for mixtures of grains of two sizes at different proportions of these grains number. The spectra of traction forces are described by the power relations.

It is found out that the action by weak periodic waves with distinct frequencies on the

granular medium which is in the state of shear deformation affect the medium's state. There exists the frequency (~ 500 Hz) when maximal effect of periodic stimulus is manifested. The experiments have also shown that acting on the medium with small perturbations when the force of tension of a certain threshold value can be achieved, it is possible to attain smoother deformation. They also revealed that the smaller this threshold, the smoother the deformation. This indicates that the medium becomes smoother.

Finally, it should be noted that the detection of statistical regularities described by power laws testify that the granular medium evolves in the state of self-organized criticality. This state has quantitative characteristics which are similar to phenomena in seismic zones. This similarity can open new perspectives to control the seismically active zones due to the possibilities to affect the nonequilibrium block medium via the weak loading.

References

- [1] Alexeevskaya, M., Gabrielov, A., Gelfand I., Gvishiani, A., & Rantsman, E. (1977). Formal morphostructural zoning of mountain territories. *Journal of Geophysics*, 43, 227–233.
- [2] Gabrielov, A.M., Keilis-Borok, V.I., Levshina, T.A., & Shaposhnikov, V.A. (1986). Block model of dynamics of the lithosphere. *Computational Seismology*, 19, 168–177.
- [3] Keilis-Borok, V.I. (1990). The lithosphere of the Earth as a nonlinear system with implications for earthquake prediction. *Reviews of Geophysics*, 28(1), 19–34.
- [4] Keilis-Borok, V.I., & Soloviev, A.A. (2003). *Nonlinear Dynamics of the Lithosphere and Earthquake Prediction*. Berlin: Springer.
- [5] Ben-Zion, Y. (2008). Collective behavior of earthquakes and faults: Continuum-discrete transitions, progressive evolutionary changes, and different dynamic regimes. *Reviews of Geophysics*, 46, RG4006. <https://doi.org/10.1029/2008RG000260>
- [6] Sadoskiy, MA, Pisarenko, V.F., & Rodionov, V.N. (1983). From seismology to geomechanics. On the model of the geophysical medium. *Bull. USSR Acad. Sci.*, 1, 82–88.
- [7] Meade, B.J., Hager, B.H., & King, R.W. (2002). Block models of present day deformation in Southern California constrained by geodetic measurements. *Proceedings and Abstracts of SCEC Annual Meeting, USA*, 96.
- [8] Billi, A., Salvini, F., & Storti, F. (2003). Fractal distribution of particle size in carbonate cataclastic rocks from the core of a regional strike-slip fault zone. *Journal of Structural Geology*, 25, 1779–1794.
- [9] Billi, A., & Storti, F. (2004). Fractal distribution of particle size in carbonate cataclastic rocks from the core of a regional strike-slip fault zone. *Tectonophysics* 384, 115–128.
- [10] McCaffrey, R. (2005). Block kinematics of the Pacific-North America plate boundary in the southwestern United States from inversion of GPS, seismological, and geologic data. *Journal of Geophysical Research*, 110, B07401. <https://doi.org/10.1029/2004JB003307>

- [11] Becker, T.W., Hardebeck, J.L., & Anderson, G. (2005). Constraints on fault slip rates of the southern California plate boundary from GPS velocity and stress inversions. *Geophysical Journal International*, 160, 634-650 <https://doi.org/10.1111/j.1365-246X.2004.02528.x>
- [12] Loveless, J.P., & Meade, B.J. (2011). Stress modulation on the San Andreas Fault by interseismic fault system interactions. *Geology*, 39(11), 1035-1038. <https://doi.org/10.1130/G32215.1>
- [13] Meroz, Y., & Meade, B.J. (2017). Intermittent Granular Dynamics at a Seismogenic Plate Boundary. *Physical Review Letters*, 119, 138501. <https://doi.org/10.1103/PhysRevLett.119.138501>
- [14] Bak, P., & Tang, C. (1989). Earthquakes as a self-organized critical phenomenon. *Journal of Geophysical Research*, 94 (B11), 15635-15637.
- [15] Sornette, A., & Sornette, D. (1989). Self-Organized Criticality and Earthquakes. *Europhysics Letters*, 9(3), 197-202. <https://doi.org/10.1209/0295-5075/9/3/002>
- [16] Bak, P., C. Tang, & K. Wiesenfeld, (1987). Self-organized criticality: An explanation of 1/f noise. *Physical Review Letters*, 59, 381-384.
- [17] Ito, K., & Matsuzaki, M. (1990). Earthquakes as Self-Organized Critical Phenomena. *Journal of Geophysical Research*, 95(B5), 6853-6860.
- [18] Nakanishi, H. (1990). Cellular-automaton model of earthquakes with deterministic dynamics. *Physical Review A*, 41, 7086-7089. <https://doi.org/10.1103/PhysRevA.41.7086>
- [19] Barriere, B., & Turcotte, D.L. (1991). A scale-invariant cellular-automata model for distributed seismicity. *Geophysical Research Letters*, 18(11), 2011-2014.
- [20] Ito, K. (1992). Towards a new view of earthquake phenomena. *Pure and Applied Geophysics*, 138, 531-548.
- [21] Olami, Z., Feder, H.J.S., & Christensen K. (1992). Self-Organized Criticality in a Continuous, Nonconservative Cellular Automaton Modeling Earthquakes. *Physical Review Letters*, 68(8), 1244-1247.
- [22] Barriere, B., & Turcotte, D.L. (1994). Seismicity and self-organized criticality. *Physical Review E*, 49(2), 1151-1160.
- [23] Baiesi, M. (2009). Correlated earthquakes in a self-organized model. *Nonlinear Processes in Geophysics*, 16, 233-240.
- [24] Kiyashchenko, D., Smirnova, N., Troyan, V., Saenger, E., & Vallianatos, F. (2004). Seismic hazard precursory evolution: fractal and multifractal aspects. *Physics & Chemistry of the Earth*, 29, 367-378.
- [25] Uritsky, V., Smirnova, N., Troyan, V., & Vallianatos, F. (2004). Critical dynamics of fractal fault systems and its role in the generation of pre-seismic electromagnetic emissions. *Physics & Chemistry of the Earth*, 29, 473-480.

- [26] Burridge, R., & Knopoff, L. (1967). Model and theoretical seismicity, *Bulletin of the Seismological Society of America*, 57, 341-371.
- [27] Carlson, J. M., & Langer, J. S. (1989). Properties of earthquakes generated by fault dynamics. *Physical Review Letters*, 62, 2632–2635.
- [28] Carlson, J. M., & Langer, J. S. (1989). Mechanical model of an earthquake fault, *Physical Review A*, 40, 6470–6484.
- [29] Christensen, K., & Olami, Z. (1992). Variation of the Gutenberg-Richter b-values and nontrivial temporal correlations in a spring-block model for earthquakes. *Journal of Geophysical Research*, 97, 8729–8735.
- [30] Christensen, K., & Olami, Z. (1992). Scaling, phase transitions, and nonuniversality in a self-organized critical cellular automaton model. *Physical Review A*, 46, 1829–1838.
- [31] Hainzl, S., Zoller, G., & Kurths, J. (1999). Similar power laws for foreshock and aftershock sequences in a spring-block model for earthquakes. *Journal of Geophysical Research*, 104(B4), 7243–7253. DOI:10.1029/1998JB900122.
- [32] Mykulyak S.V. (2018). Hierarchical block model for earthquakes. *Physical Review E*, 97, 062130.
- [33] Danylenko, V. A., Mykulyak, S.V., Polyakovskiy O.V., Kulich, V.V. , & Oleynik, I.I. (2017). Force distribution in a granular medium under dynamic loading *Physical Review E*, 96, 012906.
- [34] Behringer, R.P., Howell, D., Kondic, L., Tennakoon, S., & Veje, C. (1999). Predictability and granular materials. *Physica D*, 133, 1-17.
- [35] Howell, D., Behringer, R.P., & Veje, C. (1999). Stress fluctuations in a 2D granular Couette experiment: a continuous transition. *Physical Review Letters*, 82(26), 5241-5244.
- [36] Cabalar, A.F. (2015). Stress fluctuations in granular material response during cyclic direct shear test. *Granular Matter*, 17(4), 439-446.
- [37] Mykulyak, S., Kulich, V., & Skurativskiy, S. (2019). Simulation of shear motion of angular grains massif via the discrete element method. In: Hu, Z., Petoukhov, S., Dychka, I., He, M. (eds.) *Advances in Intelligent Systems and Computing*, (pp. 74-81), Springer.
- [38] Zhao, D., Nezami, E.G., Hashash, Y.M.A., & Ghaboussi, J. (2006). Three-dimensional discrete element simulation for granular materials. *Engineering Computations*, 23, 749-770.
- [39] Indraratna, B., Ngo, N., Rujikiatkamjorn, C., & Vinod, J. (2014). Behavior of fresh and fouled railway ballast subjected to direct shear testing: discrete element simulation. *International Journal of Geomechanics*, 14(1), 34-44.

- [40] Meroz, Y., & Meade, B.J. (2017). Intermittent granular dynamics at a seismogenic plate boundary. *Physical Review Letters*, 119, 138501.
- [41] Howell D. W., Behringer R. P., Veje C. T. (1999). Fluctuations in granular media. *Chaos*, 9(3), 559-572.
- [42] Roding, M. (2017). Shape-dependent effective diffusivity in packings of hard cubes and cuboids compared with spheres and ellipsoids. *Soft Matter*, 13, 8864-8870.
- [43] Leonard, M., and B. L. N. Kennett (1999). Multi-component autoregressive techniques for the analysis of seismograms, *Phys. Earth Planet. Int.* 113(2), 247-264.
- [44] Leonard, M. (2000). Comparison of manual and automatic onset time picking. *Bull. Seismol. Soc. Am*, 90(6), 1384-1390.
- [45] Trifunac, M. D. & Brady, A. G. (1975). A study on the duration of strong earthquake ground motion. *Bulletin of the Seismological Society of America*, 65(3), 581-626.
- [46] Gutenberg, R., & Richter, C. (1944). Frequency of earthquakes in California, *Bull. Seismol. Soc. Am.*, 34, 185-188.
- [47] Jones L.M, & Molnar P. (1979). Some characteristics of foreshocks and their possible relationship to earthquake prediction and premonitory slip on faults, *Journal of Geophysical Research: Solid Earth*, 84(B7), 3596-3608.
- [48] Omori, F. (1894) On the aftershocks of earthquakes. *Journal of the College of Science, Imperial University of Tokyo*, 7, 111-120.
- [49] Utsu, T. (1969). Aftershocks and earthquake statistics (I). *Journal of the Faculty of Science, Hokkaido University, Series 7*, 3(3), 129-195.
- [50] Vallianatos, F., Benson, P., Meredith P., & Sammonds, P. (2012). Experimental evidence of a non-extensive statistical physics behavior of fracture in triaxially deformed Etna basalt using acoustic emissions. *European Physical Journal*, 97, 58002.
- [51] Vallianatos, F., & Telesca, L. (2012). Statistical mechanics in earth physics and natural hazards (editorial), *Acta Geophysica*, 60(3), 499-501.
- [52] Vallianatos, F., & Sammonds, P. (2013). Evidence of non-extensive statistical physics of the lithospheric instability approaching the 2004 Sumatran-Andaman and 2011 Honshu mega-earthquakes, *Tectonophysics*, 590, 52-58.
- [53] Vallianatos, F., Michas, G., Benson, P., & Sammonds, P. (2013). Natural time analysis of critical phenomena: The case of acoustic emissions in triaxially deformed Etna basalt, *Physica A: Statistical Mechanics and its Applications*, 392(20), 5172-5178.
- [54] Michas, G. Vallianatos, F., & Sammonds, P. (2013). Non-extensivity and long-range correlations in the earthquake activity at the West Corinth rift (Greece). *Nonlinear Processes Geophysics*, 20, 713-724.

- [55] Vallianatos, F., Karakostas, V., & Papadimitriou, E. (2014). A non-extensive statistical physics view in the spatiotemporal properties of the 2003 (Mw6.2) Lefkada, Ionian Island Greece, aftershock sequence. *Pure and Applied Geophysics*, 171(7), 1343–1534. DOI: 10.1007/s00024-013-0706-6.
- [56] Michas, G., Vallianatos, F., & Sammonds P. (2015). Statistical mechanics and scaling of fault population with increasing strain in the Corinth Rift. *Earth and Planetary Science Letters*, 431, 150–163.
- [57] Vallianatos, F., Michas, G., & Papadakis, G. (2015). A description of seismicity based on non-extensive statistical physics: a review. In: *Earthquakes and Their Impact on Society*, (p.1-41), Series Title: Springer Natural Hazard, Springer.
- [58] Agioutantis, Z., Kaklis, K., Mavigiannakis, S., Verigakis, M., Vallianatos, F., & Saltas, V. (2016). Potential of acoustic emissions from three point bending tests as rock failure precursors. *International Journal of Mining Science and Technology*, 26(1), 155–160.
- [59] Hloupis, G., Stavrakas, I., Vallianatos, F., & Triantis, D. (2016). A preliminary study for prefailure indicators in acoustic emissions using wavelets and natural time analysis, *Proceedings of the Institution of Mechanical Engineers, Part L: Journal of Materials: Design and Applications*, 230(3), 780-788.
- [60] Vallianatos, F., Papadakis, G., & Michas, G. (2016). Generalized statistical mechanics approaches to earthquakes and tectonics. *Proceedings of the Royal Society A*, 472, 2196.
- [61] Kaklis, K., Saltas, V., Mavrigiannakis, S., Vallianatos, F., & Agioutantis, Z. (2017). Using Acoustic Emissions to enhance Fracture Toughness Calculations for CCNBD Marble Specimens, *Fracture and Structural Integrity*, 40, 117.
- [62] Vallianatos, F., Michas, G., & Papadakis, G. (2018). Non extensive statistical seismology: an overview. In: Chelidze, T., Telesca, L., & Vallianatos, F., *Complexity of seismic time series; Measurement and Application*, (p.25-59), Elsevier.
- [63] Saltas, V., Vallianatos, F., Triantis, D., & Stavrakas, I. (2018). Complexity in laboratory seismology: from electrical and acoustic emissions to fracture. In: Chelidze, T., Telesca, L., & Vallianatos, F., *Complexity of seismic time series; Measurement and Application*, (p.239–273), Elsevier.
- [64] Tsallis C. (2004). Nonextensive statistical mechanics : construction and physical interpretation. In: M. Gell-Mann, C.Tsallis (eds.), *Nonextensive Entropy: Interdisciplinary Applications*, (p.1-53), Santa Fe Institute Studies on the Sciences of Complexity, Oxford University Press.
- [65] Boghosian, B.M. (1996). Thermodynamic description of the relaxation of two - dimensional turbulence using Tsallis statistics. *Physical Review E*, 53(5), 4754-4763.
- [66] Ramirez-Reyes, A., Raul Hernandez-Montoya A., Herrera-Corral G., & Dominguez-Jimenez I. (2016). Determining the entropic index q of Tsallis entropy in images through redundancy. *Entropy*, 18, 299(14).